Environ. Sci. Technol. **2009,** *43,* 1192–1198

Density Functional Theory Studies of Chloroethene Adsorption on Zerovalent Iron

DONG-HEE LIM,[†]
CHRISTIAN M. LASTOSKIE,*[,†]
ALOYSIUS SOON,[‡] AND UDO BECKER[§]
Department of Civil and Environmental Engineering, University of Michigan, 1351 Beal Avenue, Ann Arbor, Michigan 48109-2125, School of Physics, University of Sydney, Sydney, New South Wales 2006, Australia, and Department of Geological Sciences, University of Michigan, 1100 North University Avenue, Ann Arbor, Michigan, 48109-1005

Received September 16, 2008. Revised manuscript received November 17, 2008. Accepted November 18, 2008.

Adsorption of perchloroethene (PCE), trichloroethene (TCE), and *cis*-dichloroethene (*cis*-DCE) on zerovalent iron is investigated using density functional theory (DFT) to evaluate hypotheses concerning the relative reactivity of these compounds on zerovalent iron. Four different chloroethene adsorption modes on the Fe(110) surface were studied using periodic DFT and the generalized gradient approximation (GGA). Of the adsorption sites examined, the atop site, where the chloroethene C═C bond straddles a surface iron atom, was the most energetically favorable site for the adsorption of all three chloroethenes. Electronic structure and property analyses provide an indication of the extent of sp^2-sp^3 hybridization. The strong hybridization of the π-bonding orbital between the chloroethene C═C bond and the iron surface suggests that adsorbed chloroethenes are strongly activated on Fe(110) and are likely precursors for subsequent chloroethene dissociation on the Fe surface. When the effect of solvation is indirectly taken into account in the DFT simulations by considering the hydration energies of chloroethenes in bulk water, the ordering of the adsorption energies of chloroethenes from the aqueous phase onto Fe(110) is in agreement with experimental observation (PCE > TCE > *cis*-DCE). Electronic properties of the adsorbed configurations of chloroethenes are also presented.

Introduction

Chlorinated solvents such as perchloroethene (PCE, C_2Cl_4), trichloroethene (TCE, C_2HCl_3), and *cis*-dichloroethene (*cis*-DCE, $C_2H_2Cl_2$) are common groundwater contaminants. PCE and TCE are among the most frequently detected contaminants at hazardous waste disposal sites due to their widespread production, use, and disposal (*1, 2*), and they cause irritation of the skin, eyes, kidneys, and respiratory tract. Moreover, TCE is suspected to be a human carcinogen (*3*). Chloroethenes released into the subsurface penetrate into the water table and persist as long-term groundwater pollutants (*4, 5*).

* Corresponding author phone: (734) 647-7940; fax: (734) 763-2275; e-mail: cmlasto@umich.edu.
[†] Department of Civil and Environmental Engineering, University of Michigan.
[‡] University of Sydney.
[§] Department of Geological Sciences, University of Michigan.

Recently, zerovalent iron (Fe^0) has gained widespread acceptance as an effective reducing agent for groundwater remediation at sites contaminated with chloroethenes (*6*−*8*), on account of its low cost and nontoxicity (*9*). The mechanisms by which iron decomposes chlorinated solvents, by cleavage of the carbon−chlorine bond (*9*), are as yet not well understood. To develop process models for the optimal design of in situ and ex situ zerovalent iron treatment systems for the removal of chlorinated solvents from drinking water supplies, it is important to understand these mechanisms, and in particular how the degree of chlorination of the contaminant affects its reactivity on the iron surface (*10*). Generally, it is assumed that reactivity should increase with increasing chlorination (*6*). For example, the dechlorination rate of PCE was reported to be 5.4 times faster on zerovalent iron (*11, 12*) and 170.2 times faster on zerovalent zinc (*10*) than that of TCE. A higher degree of chlorination was also found to favor rapid dechlorination on iron-bearing soil minerals such as biotite (*13*), magnetite (*14*), and green rust (*15*).

However, the opposite trend has also been reported for decomposition of chloroethenes by iron (*6*), with a measured overall order of reactivity for chloroethene reduction by zerovalent iron given as vinyl chloride (VC) > *cis*-DCE > TCE > PCE (*6*). A similar ordering was obtained for dechlorination of chloroethenes by palladium metal catalysts (Pd/Al) with hydrogen gas (*16*). In another study, TCE was transformed 2.6 times faster than PCE by iron sulfide (*17*). Hence, contradictory results have been reported for the reactivity ordering with respect to degree of chlorination for chloroethene reduction on metals and metal-containing minerals.

Various explanations have been offered for the conflicting results for chloroethene reactivity on zerovalent iron. One possibility is that carbon impurities within the iron may serve as nonreactive sites on the iron surface where chloroethenes may adsorb without further reaction. The adsorbed chloroethene may thus be misinterpreted as a part of the overall reaction rate (*18*). Highly chlorinated species such as PCE have a greater propensity to adsorb on carbon than less-chlorinated congeners, and this adsorption may easily be mistaken for rapid reaction (*6, 18*). However, because of the difficulty in performing quantitatively accurate experiments, it remains unresolved how the degree of chlorination affects the relative reactivity of chloroethenes on iron surfaces.

In the studies reported herein, density functional theory (DFT) methods were applied to investigate the adsorption configurations of chloroethenes on the Fe(110) surface. This was done as a first step toward elucidating the effect of chlorination on the relative reactivity of chloroethenes on zerovalent iron. Reductive dechlorination of chloroethenes may occur by a three-step process, involving adsorption of the chloroethene onto the iron surface; a surface-catalyzed reduction; and desorption of the dechlorinated product species from the surface (*6*). To determine the relative reactivity of chloroethene congeners on zerovalent iron, differentiation between the adsorption and dechlorination steps is needed so as to prevent misinterpretation of chloroethene adsorption as a part of the overall dechlorination rate. Since chemical reactions between chloroethenes and the iron surface are initiated after the molecules have adsorbed, accurate characterization of the adsorption sites and energies is an important initial step toward analyzing the surface dechlorination pathways of chloroethenes bound to zerovalent iron (*19*). In this paper, we therefore present and discuss theoretical results from DFT calculations for the adsorption energies and electronic properties of chloro-

10.1021/es802523a CCC: $40.75 © 2009 American Chemical Society
Published on Web 01/22/2009

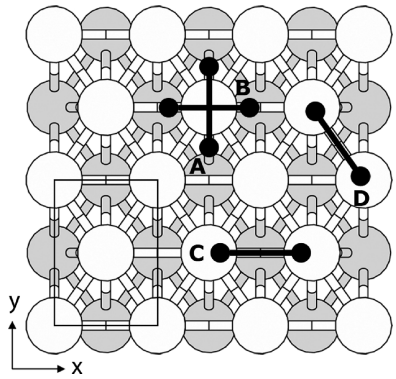

FIGURE 1. Fe(110)-*p*(3×2) supercell and adsorption sites used for chloroethene adsorption calculations. The rectangle demarcates *p*(1×1) and the solid line denotes the orientation of the chloroethene C═C bond. The lighter and darker atoms represent the surface and subsurface layers of Fe(110), respectively. (A) Atop 1 site, (B) atop 2 site, (C) long-bridge (LB) site, (D) short-bridge (SB) site.

ethenes adsorbed on the Fe(110) surface. Additionally, partial hydration energies for chloroethenes on pristine iron surfaces are used to indirectly account for solvent effects in quantum mechanical calculations. Lastly, the limitations of the pristine iron model system used in this study are noted with regard to interpretation of experimental results for aqueous phase reduction of chloroethenes on in situ iron surfaces.

Computational Methods

Adsorption Calculations using Periodic Boundary Conditions. All electronic structure calculations were performed using periodic density functional theory and the ultrasoft Vanderbilt pseudopotential method (*20*) within the generalized gradient approximation (GGA) by Perdew, Burke, and Ernzerhof (PBE) (*21*) for the exchange-correlation functional as implemented in the Plane-Wave Self-Consistent Field (PWscf) code in the Quantum-ESPRESSO open-source distribution (*22*). Kinetic-energy cutoffs for wave functions and for charge density and potential were 340.1 eV (25 Ryd) and 2449.0 eV (180 Ryd), respectively; this converges the total energy to within 0.01 eV/atom. The Monkhorst−Pack scheme (*23*) was used for the **k**-point sampling. Using a 10×10×10 **k**-point grid, the following physical properties were calculated for ferromagnetic bcc iron: equilibrium lattice constant a_0 = 2.8606 Å; bulk modulus B = 167 GPa; and magnetic moment M = 2.45 μ_B. These results are in good agreement with experimental results (*24*) for ferromagnetic bcc iron: a_0 = 2.8664 Å, B = 168 GPa, M = 2.22 μ_B.

Fe(110) is the closest-packed surface of body-centered cubic (bcc) iron. It is essentially bulk-terminated, with very little relaxation and no reconstruction (*25*). $p(2\times2)$, $p(3\times2)$, and $p(4\times2)$ supercells of Fe(110) were modeled using periodic three-layer slabs with chloroethenes (PCE, TCE, or *cis*-DCE) adsorbed on both sides of the slabs (see Supporting Information: periodic three-layer slab model in Computational Methods). This double-sided adsorption model minimizes the dipole moment perpendicular to the surface that is produced by charge rearrangement on the surface due to adsorption. The outermost layers (surface layers) of the slab were allowed to relax, whereas the center layer (below the surface) was kept rigid to represent the underlying bulk iron. The coverages of each adsorbate molecule were 0.125, 0.083, and 0.063 monolayers (ML), respectively, for the $p(2\times2)$, $p(3\times2)$, and $p(4\times2)$ supercells. The periodic cell lengths of the $p(3\times2)$ and $p(4\times2)$ supercells are 1.5 and 2 times that of the $p(2\times2)$ supercell, respectively, in the x-direction (Figure 1). The slabs were separated from their periodic images in the z-direction by a vacuum space of 16 Å. Brillouin-zone integrations were performed on a 2×3×1 Monkhorst−Pack grid of **k**-points for the Fe(110) supercells. The 2×3×1 **k**-point grid yielded adsorption energies close (less than 2.2 kJ/mol underestimation) to those obtained using the more computationally expensive 5×5×1 **k**-point grid.

Chloroethene adsorption was considered at four different candidate adsorption sites and orientations. These are the atop 1, atop 2, long-bridge (LB), and short-bridge (SB) sites shown in Figure 1. The adsorption energy (E_{ads}) per chloroethene molecule adsorbed to the iron surface is calculated as

$$E_{ads} = \frac{1}{N_{adsorbate}}[E_{adsorbate/surface} - (N_{adsorbate} \times E_{adsorbate} + E_{surface})] \quad (1)$$

where $N_{adsorbate}$ is the number of chloroethene molecules in the model system, and $E_{adsorbate/surface}$, $E_{adsorbate}$, and $E_{surface}$ represent the total energies of the chloroethene/iron system, the free chloroethene molecule, and the clean iron surface, respectively. The geometry of the free adsorbate molecule was optimized in a 12 Å cubic box, where little interaction is expected between the gas phase chloroethene and its periodic images. A negative adsorption energy indicates that adsorption is exothermic (stable) with respect to the free adsorbate molecule.

Geometry optimizations are halted when the forces acting on each relaxed atom of the system were smaller than a relatively lax convergence criterion of 5.14×10^{-1} eV/Å (2×10^{-2} Ryd/a.u.), as noted in the Supporting Information, Figure S1. The optimized structures were visualized using the XCrySDen graphical package (*26*).

Cluster Model Analysis. After obtaining the adsorbed chloroethene configurations from periodic slab calculations using Quantum-ESPRESSO, the coordinates of the adsorbed chloroethenes and neighboring iron surface atoms were transferred to Gaussian 03 (*27*) to calculate single point energies and to identify important bonding orbitals between the C═C bond and the Fe surface. The GGA of PBE for the exchange-correlation functional was used with the Los Alamos LanL2DZ double-ζ basis set. Molecular orbitals are visualized using the MOLDEN molecular density viewer (*28*). Hydration energies of the chloroethenes are calculated using the polarized continuum model (PCM) (*29*) implemented in Gaussian 03 with the same functional method and basis set as used in the bonding orbital analyses.

Results and Discussion

Effect of Supercell Size and k-point Grid on Adsorption. To design a proper iron surface model, the effect of supercell size was studied for the $p(2\times2)$, $p(3\times2)$, and $p(4\times2)$ supercells of Fe(110) with adsorbates at the atop 1 site. This site was selected for analysis because it exhibited the most energetically favorable adsorption configurations for chloroethenes in a preliminary study using the Fe(110)-$p(2\times2)$ supercell with a fixed iron surface layer (data not shown here). The $p(3\times2)$ supercell was found to be a reasonable supercell size for obtaining property results comparable to larger supercells while reducing the computational burden associated with the DFT calculations (see Supporting Information, Figure S2). The adsorption energies of the chloroethenes on the Fe(110) atop 1 site decrease (i.e., become more exothermic) with increasing supercell size, as repulsive interactions between the adsorbate and its periodic images are reduced. A similar trend was observed for oxygen adsorption on Cu(111) as coverage was varied (*30*). In addition, adorption at the LB and SB sites of the Fe(110)-$p(2\times2)$ supercell with a fixed surface yielded endothermic (unstable) chloroethene adsorption energies (data not shown here). Although the adsorption energy on the fixed $p(2\times2)$ supercell surface is

TABLE 1. Adsorption Enegies and Geometry of Chloroethenes Adsorbed on the Fe(110)-$p(3\times2)$ Surfaces in the Gas Phase[a]

Hydration energy (kJ/mol)		adsorption energy[b] (kJ/mol)				geometry of chloroethenes[c] (bond (Å), angle (°))			
		atop 1	atop 2	LB	SB	C=C	C—Cl	C—H	dihedral angle
PCE[d]	−4.5	−69.7	−60.9	−12.0	−44.7	1.480	1.857		122.0
TCE	−13.1						1.822[f] (1.713[f])		131.9[h]
		−69.2 (−62.6)	−56.4 (−49.8)	−17.8 (−11.3)	−49.7 (−43.1)	1.460 (1.346)	1.829[g] (1.715[g]) 1.850 (1.727)	1.103 (1.091)	(180.0[h]) 122.6[i] (180.0[i])
cis-DCE[e]	−24.0	−66.5 (−54.5)	−43.1 (−31.1)	−21.5 (−27.4)	−39.4 (−9.5)	1.478 (1.340)	1.857 (1.716)	1.113 (1.092)	124.9 (180.0)

[a] Adsorption energies in the aqueous phase[b] and geometries of chloroethenes in the gas phase[c] are shown in parentheses. [b] Values in parentheses are adsorption energies for aqueous-phase chloroethenes, calculated assuming a 50% partial hydration for chloroethenes adsorbed on the iron surface. [c] Values in parentheses are geometries of chloroethenes in the gas phase. [d] PCE geometry is symmetric about the center of the C=C bond. [e] *cis*-DCE geometry is symmetric about the centerline perpendicular to the C=C bond. [f] C—Cl bond on the carbon bonded to a hydrogen atom. [g] C—Cl bond diagonal to the C—H bond. [h] Cl—C—C—Cl dihedral angle. [i] H—C—C—Cl dihedral angle.

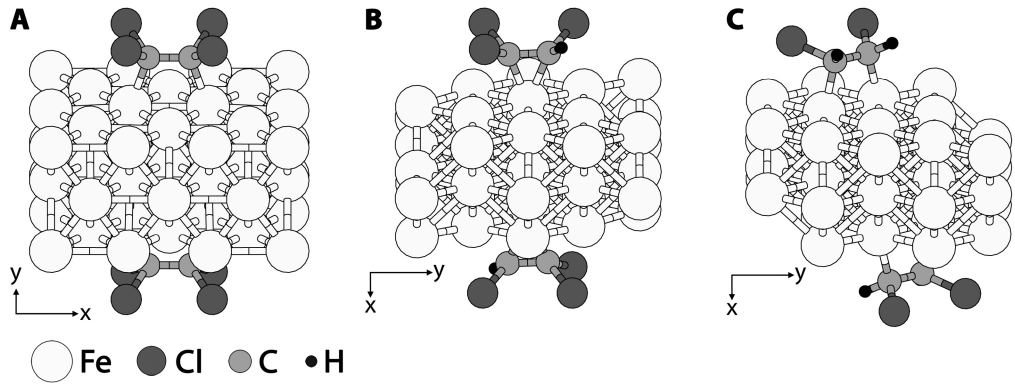

FIGURE 2. Adsorbed configurations of PCE, TCE, and *cis*-DCE on the relaxed Fe(110)-$p(3\times2)$ surface. (A) PCE at long-bridge (LB). (B) TCE at atop 1. (C) *cis*-DCE at short-bridge (SB) (more adsorption configurations available in Supporting Information Figure S4).

less than 9 kJ/mol larger than that for the relaxed $p(2\times2)$ surface (Supporting Information Figure S2), the size of the $p(2\times2)$ supercell is insufficient to determine chloroethene adsorption energies because of repulsive interactions between the periodic images of these relatively large adsorbates on the iron surface.

The effect of the **k**-point grid size was also sampled to determine a suitable **k**-point grid for the adsorption studies, the adsorption energies of chloroethenes at atop 1 site of the Fe(110)-$p(3\times2)$ supercell were calculated for a selection of different **k**-point grids. Adsorption energies for PCE, TCE, and *cis*-DCE are shown relative to the energies obtained for the $5\times5\times1$ **k**-point grid in Supporting Information Figure S3. A coarser grid, $2\times3\times1$, yields sorption energies close to those of the $5\times5\times1$ **k**-point grid, with less than 2.2 kJ/mol difference from the baseline energies from all three chloroethenes. Moreover, the ordering of the adsorption energies of PCE, TCE, and *cis*-DCE is unchanged when the smaller $3\times3\times1$ and $2\times3\times1$ **k**-point grids are used instead of the larger and more computationally expensive $5\times5\times1$ and $7\times7\times1$ grids. Therefore, in this study, the $2\times3\times1$ **k**-point grid was used to calculate the chloroethene adsorption energies and activation energies.

Chloroethene Adsorption on Fe(110)-$p(3\times2)$. Surface relaxation of the three-layered clean Fe(110) slab was carried out and the final geometry was compared with experimental data to verify the iron surface model. Lateral relaxation of Fe atoms in the *x*- and *y*-direction was 0.008% and 0.007%, respectively, relative to the distance between Fe atoms in the fixed surface model. This was negligible compared with relaxation normal to the surface (i.e., in the *z*-direction) and indicates that the Fe(110) surface does not reconstruct, in agreement with experimental and theoretical results (*24*, *31*, *32*). Surface relaxation is determined by measuring the distance the first layer moves (δz). A positive and a negative value represent expansion and contraction of the surface layer, respectively. The average relaxation δz of the surface Fe(110) atoms as a percentage of the interlayer spacing was −0.15, where the negative value indicates contraction of the surface layer toward the subsurface layer (3×10^{-3} Å contraction). This is in agreement with a quantum mechanical study ($\delta z = -0.13$) (*32*) and falls within the range reported from experimental measurement ($\delta z = +0.5 \pm 2$) (*31*).

Chloroethenes with gas-phase optimized geometries were placed on the four adsorption sites (atop 1, atop 2, LB, and SB) shown in Figure 1 of relaxed-surface Fe(110)-$p(3\times2)$ and reoptimized to calculate the adsorption energies. As indicated in Table 1, the atop 1 site exhibits the most energetically favorable adsorption configuration for all three chloroethenes investigated, with adsorption energies on this site that are 9−58 kJ/mol more negative than those of other adsorption sites. The adsorbed configurations of PCE, TCE, and *cis*-DCE, shown in Figure 2 (see also Supporting Information Figure S4), deviate significantly from their planar gas phase geometries. The C=C bond approaches the Fe surface to within 1.85−1.91 Å, whereas the C—Cl and C—H bonds deflect away from the surface. The latter is reflected in a reduction of the 180.0° gas-phase chloroethene Cl—C—C—Cl dihedral angle to 122.0° to 131.9° for chloroethenes adsorbed on the Fe(110) surface (Table 1). Also, the C=C bond and C—Cl

bonds of adsorbed chloroethenes are elongated by 0.11−0.14 Å relative to their gas-phase geometries (Table 1).

The adsorbed configurations thus reveal sp^2−sp^3 hybridization of the chloroethene carbon atoms, in agreement with the adsorption geometry found for TCE on PdCu(110) (*33*). The geometry changes of the adsorbed chloroethenes demonstrate strong activation for dechlorination on the Fe(110) surface. Similar structural changes were reported in the adsorption of ethylene (C_2H_4) on various metal surfaces (*34*−*39*). Bernardo and Gomes (*34*) suggest that the adsorption of ethylene occurs mainly on the atop site of Cu(110), Ag(110), and Pt(110) surfaces, indicating carbon−carbon bond elongation. This bond elongation, accompanied by partial hybridization toward the sp^3 configuration, is a common phenomenon in the adsorption of ethylene on Ag(100) (*35*), Pd(110) (*36*), Pt(111) (*37*), Ag(111) (*38*), and Pd(111) (*39*). Zhang et al. (*40*), however, reported a C═C bond contraction by 0.043 Å upon adsorption of TCE on the most energetically favorable site of Fe(100). This is probably because the C−Cl bonds are highly elongated (3.418 Å), such that the adsorbed TCE molecule acts as if it is in a dissociated configuration, with very little overlap in electron density between the C and Cl atoms and a C═C bond that is closer in character to a C≡C triple bond. The highly activated adsorbed TCE molecule reported by Zhang et al. (*40*) has a much larger adsorption energy (−691 kJ/mol) than the result obtained in this work (−69.7 kJ/mol) for TCE on Fe(110). It should be noted that the Fe(100) surface investigated by Zhang et al. (*40*) is a more open, low-density surface than Fe(110). Low-density crystal faces of transition metals are known to be much more active than close-packed surfaces (*41*).

The adsorbed configurations of the chloroethenes may directly affect the relative activation energies among the different possible dechlorination pathways. The C−Cl bond length (1.850 Å) on the CCl_2 group of TCE is, for example, more elongated, and hence more activated for dechlorination, than that of the CHCl group (C−Cl bond elongation of 1.822 Å). Barbosa and Sautet (*42*) similarly report that C−Cl bond dissociation of TCE is more favorable from the CCl_2 group than the CHCl group.

Hydration Energy. For investigation of adsorption and dissociation of chloroethenes on zerovalent iron in groundwater remediation applications, it is important, albeit challenging, to take into account solvent effects in quantum mechanical simulations of metal surface-catalyzed reactions. The thermodynamics and kinetics of surface reactions can be significantly modified in the presence of a solvent because partially charged intermediates that are unstable in the gas phase can exist in solution and participate in the reactions (*40, 43*). However, explicit inclusion of solvent effects in quantum mechanical simulations requires huge computational resources, especially when relatively large adsorbate molecules are investigated on transition metal surfaces such as in this study. Thus, only the hydration energies of chloroethene molecules in bulk water are used in this study to take solvent effects into account. Explicit calculation of the partial hydration of the adsorbate on the surface is neglected because of the computational expense of calculating the hydration of the entire iron-chloroethene cluster. The adsorption energy in the presence of water can be approximated by calculating adsorption in the gas phase and correcting for the loss in hydration energy of the chloroethenes.

The hydration energies of PCE, TCE, and *cis*-DCE calculated using the PCM method as implemented in Gaussian 03 (*27*) are −4.5, −13.1, and −24.0 kJ/mol (Table 1). Since the enthalpy of hydration of the hydrogen ion (−1106.7 kJ/mol) is more negative, due to the formation of hydrogen bonds, than that of the chlorine ion (−340.2 kJ/mol) (*44*), hydration energy decreases as the number of hydrogen atoms increases. Negative hydration energies indicate that chloroethenes must overcome the loss of hydration energy upon adsorption, resulting in less exothermic (or more endothermic) adsorption energies from the aqueous phase. To estimate the hydration energies of the adsorbed species, Becker and coworkers (*45*) used molecular dynamics simulations to determine the adsorption energies of species on sulfate surfaces. They determined that the hydration energy of a Ba^{2+} ion on a corner site of the Barite ($BaSO_4$) surface is about 20% of the Ba^{2+} hydration energy in bulk water (*45*). This is because the ion is less exposed to solvent water in the corner adsorption site. For a chloroethene molecule adsorbed on a planar Fe(110) surface, it is reasonable to a first approximation to assume that the hydration energy of the adsorbed molecule is 50% of the hydration energy of the same species in bulk water. Using the gas-phase adsorption energy (E_{ads_gas}) and the bulk water hydration energy (E_{hyd_bulk}) of the chloroethene, adsorption energies from the aqueous phase (E_{ads_water}) can be calculated as

$$E_{ads\_water} = E_{ads\_gas} - (p \times E_{hyd\_bulk}) \quad (2)$$

where p is the fractional solvation of the adsorbed molecule (here assumed to be 50% or $p = 0.5$).

Adsorption energies of chloroethenes from water are reported as the values in parentheses in Table 1. PCE shows stronger adsorption from water on the Fe(110) surfaces than TCE and *cis*-DCE in agreement with experimental results showing that aqueous adsorption constants for chloroethenes increase with increasing halogenation (*6, 13*−*15, 18*). Arnold and Roberts (*6*) report similar results, although the adsorption constant they obtained for PCE is smaller than that for TCE. Lee and Batchelor (*13*−*15*) also showed that the adsorption constants of chloroethenes on reactive iron-bearing soil minerals increase with increasing chlorination. Although the magnitude of difference in adsorption energy is small (∼3 kJ/mol) among the chloroethenes in the gas phase calculation, by considering partial hydration of chloroethenes adsorbed on the Fe surface from the aqueous phase, a distinct difference (∼13 kJ/mol) in the adsorption energies of PCE and *cis*-DCE is revealed. Because hydrogen has a more negative hydration enthalpy than chlorine, the more highly halogenated chloroethenes are more strongly adsorbed to the solvated Fe surface.

It should be recognized that the surfaces of zerovalent iron in remediation environments are unlikely to be pristine metal surfaces. Rather, they are likely to be corroded, and as a result the surface layers will be covered with a film of oxide or oxyhydroxide (*46*). Chloroethenes then adsorb onto the film of oxide covering the surface, and not the pristine iron itself. This study does not explicitly simulate the Fe-oxide film. Instead, by taking into account the partial hydration energy, the interaction of water with the activated Fe−chloroethene complex is accounted for indirectly. If the partial hydration energy of chloroethenes adsorbed on the iron surface can be estimated, the correction for aqueous-phase adsorption energies, as posed in our study, is a proper method, although the results will necessarily depend on the assumed percentage of partial hydration for the adsorbed species bound to the iron. Direct calculations of chloroethene hydration energies, in the explicit presence of water, using molecular dynamics simulations may be helpful to obtain more accurate hydration energies in the adsorbed state, especially when adsorption is considered on surfaces with vacancies, steps, or kinks.

Electronic Property Analysis. To examine adsorbed configurations in detail, the projected density of states (PDOS) on d orbitals of the relaxed Fe(110)-$p(3\times2)$ surface atoms was analyzed. Valence electrons in the outermost orbitals of these atoms serve a key role in the adsorption interaction.

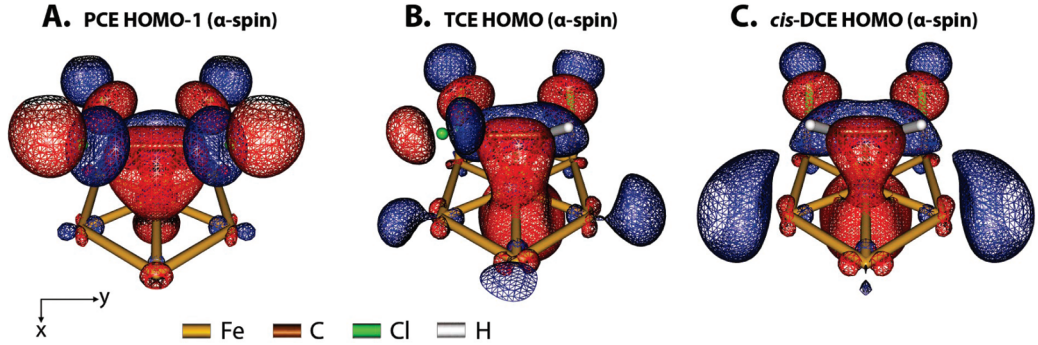

FIGURE 3. The α-spin second-highest occupied molecular orbitals (HOMO-1) of adsorbed PCE and HOMOs of adsorbed TCE and *cis*-DCE at the atop 1 site of the Fe_7 cluster model. The two colors distinguish the positive and negative portions of the wave function. (Color images are available at http://pubs.acs.org).

The PDOS on *d* orbitals of the Fe surface atoms on which chloroethenes are adsorbed (Supporting Information Figures S5C, S5D, and S5E) show broader and strongly modified bands ranging from −5 to −15 eV below the Fermi level compared to that of the clean Fe surface (Supporting Information Figure S5A). This shows that the molecular orbitals of each chloroethene strongly interact with the *d* band of the Fe atoms resulting in the mixing band region. To support this, the same PDOS calculation was performed on a relaxed Fe surface, with intact PCE placed 5 Å above the surface to prevent it from interacting with the surface (Supporting Information Figure S5B). The PDOS of the *d* orbital of the Fe surface with the noninteractive PCE is almost unchanged compared with the PDOS of the clean Fe surface (Supporting Information Figure S5A), indicating little electronic interaction between surface Fe atoms and the far-removed PCE. Thus, the interaction between the chloroethene molecular orbitals and the *d* band of the relaxed Fe(110)-$p(3\times2)$ surface atoms is responsible for the mixing band region observed in the PDOS between −5 and −15 eV below the Fermi level.

Strong hybridizations were also detected in the p_z orbitals (with the *z* direction perpendicular to the iron surface) of both carbon and chlorine in PCE adsorbed on the Fe surface (Supporting Information Figures S5G and S5I), while those of noninteractive PCE by contrast showed localized sharp peaks (Supporting Information Figure S5F and S5H). This is further evidence of the strong interaction between the chloroethene molecules and the Fe surface, with mixing bands at −14.0 eV in both Supporting Information Figures S5C and S5G, and at −9.8 and −7.8 eV in both Supporting Information Figure S5C and S5I. The broad bands of the carbon p_z orbital covering the range of Fe *d* bands represent the weakened C═C bond, as expected from the elongated C═C bond length (Table 1). A similar observation in the carbon *p* band was reported in the adsorption of acetylene on Fe(001) by Lee and co-workers (*47*). Strong hybridization could probably be attributed to the open shell $3d^6$ structure of iron that participates much more in bonding than closed shell *d* structure-atoms (e.g., $4d^{10}$ of silver and $3d^{10}$ of copper) (*34*).

In addition to the PDOS analysis, the highest occupied molecular orbitals (HOMOs) and lowest unoccupied molecular orbitals (LUMOs) of adsorbed PCE, TCE, and *cis*-DCE at the atop 1 site were analyzed using the cluster model approach as described in Computational Methods. Although the localized basis set used in the Gaussian 03 cluster model (*27*) has limitations to describe electronic properties calculated using the plane-wave basis set, the cluster approach is useful to visualize and interpret the molecular orbitals responsible for the interaction between the adsorbed chloroethenes and the iron surface.

From the adsorbed configurations of chloroethenes at atop 1 site on the Fe(110) surface (Figure 2 and Supporting Information Figure S4), hybridized bonding π-orbitals are shown in the HOMO of PCE and in the LUMOs of TCE and *cis*-DCE (see Supporting Information, Figure S6). The π-orbitals clearly contribute to hybridized bonding between PCE and the Fe surface; however, the π-orbitals of TCE and *cis*-DCE do not apprear to participate in bonding. This is most likely because the adsorbed geometries of TCE and *cis*-DCE were obtained at an early stage of adsorption; the adsorbed configurations can vary depending on the convergence criteria used in the geometry optimization (see Supporting Information Figure S1). Thus, other possible adsorbed configurations of PCE, TCE, and *cis*-DCE were analyzed to verify the π-orbitals. Figure 3 shows the α-spin highest and second-highest occupied molecular orbitals (HOMO and HOMO-1, respectively) of the adsorbed chloroethenes, calculated using the tighter convergence criteria for geometry optimization. Although the adsorbed chloroethene geometries in Figure 3 are almost identical to those shown in Figure 2 and Supporting Information Figure S4, with the tighter convergence criteria the C═C chloroethene bond in Figure 3 approaches 0.1 Å closer to the iron surface than the C═C bond in Figure 2 and Supporting Information Figure S4; and the lengths of the C═C and C—Cl chloroethene bonds are, on average, 0.02 Å shorter and 0.07 Å longer, respectively, in Figure 3 than in Figure 2 and Figure S4. The tighter convergence criteria thus yields an adsorbate geometry that is nearer to the Fe surface. Also, the hybridized bonding π-orbitals shown as the LUMOs of TCE and *cis*-DCE in Supporting Information Figure S6 are shifted below their energy levels and represent the HOMOs in Figure 3. Put another way, when the chloroethene geometry is more proximate to the surface, the π-orbitals shown in the LUMOs are filled from the transfer of *d*-electrons from the iron surface, hence becoming the HOMOs of the adsorbed TCE and *cis*-DCE configurations. Thus, hybridized bonding π-orbitals are responsible for the chloroethene adsorption on the Fe(110) surface. The *d* orbital character is also evident in the HOMOs; therefore, the interaction between the chloroethenes and the Fe surface may be characterized as $\pi-d$ orbital hybridization. This interaction can be interpreted in terms of the Dewar—Chatt—Duncanson mechanism, where the filled π molecular orbital of an alkene donates electrons to unoccupied valence *d* orbitals of metals, while other occupied *d* orbitals back-donate into the empty π^* antibonding orbital of the adsorbate double bond (*48, 49*). The π donation and π back-donation are responsible for the increase in the carbon—carbon bond distance upon adsorption that accompanies sp^2-sp^3 hybridization (*36*). Sivavec and Horney (*50*) has also proposed that strong π-bonding between chloroethenes and the iron surface may prevent desorption until dechlorination is complete.

In summary, geometric and the electronic property analyses indicate that the atop 1 adsorbed configurations on

the Fe(110) surface is the likely precursors for subsequent dissociation of chloroethenes on the Fe surface.

Acknowledgments

This research was supported by the National Science Foundation through TeraGrid resources provided by TACC and SDSC (to Christian Lastoskie), by the NSF-NIRT grant EAR-0403732 (to Udo Becker), and in part by a Rackham Graduate Student Research Grant Award from the University of Michigan (to Dong-Hee Lim). We thank Axel Kohlmeyer at the University of Pennsylvania for his helpful comments.

Supporting Information Available

Discussion of computational methods, and additional information on the adsorbed chloroethene configurations, PDOS results, and HOMO/LUMO images are available free of charge via the Internet at http://pubs.acs.org.

Literature Cited

(1) Doherty, R. E. A history of the production and use of carbon tetrachloride, tetrachloroethylene, trichloroethylene and 1,1,1-trichloroethane in the United States: Part 1—Historical background; Carbon tetrachloride and tetrachloroethylene. *Environ. Forensics* **2000**, *1* (2), 69–81.

(2) Doherty, R. E. A history of the production and use of carbon tetrachloride, tetrachloroethylene, trichloroethylene and 1,1,1-trichloroethane in the United States: Part 2—Trichloroethylene and 1,1,1-trichloroethane. *Environ. Forensics* **2000**, *1* (2), 83–93.

(3) *11th Report on Carcinogens*; Department of Health and Human Services, National Toxicology Program (NTP): Research Triangle Park, NC, 2005.

(4) Parker, B. L.; Gillham, R. W.; Cherry, J. A. Diffusive disappearance of immiscible-phase organic liquids in fractured geologic media. *Ground Water* **1994**, *32* (5), 805–820.

(5) Aggarwal, V.; Li, H.; Boyd, S. A.; Teppen, B. J. Enhanced sorption of trichloroethene by smectite clay exchanged with Cs+. *Environ. Sci. Technol.* **2006**, *40* (3), 894–899.

(6) Arnold, W. A.; Roberts, A. L. Pathways and kinetics of chlorinated ethylene and chlorinated acetylene reaction with Fe(O) particles. *Environ. Sci. Technol.* **2000**, *34* (9), 1794–1805.

(7) Orth, W. S.; Gillham, R. W. Dechlorination of trichloroethene in aqueous solution using Fe-O. *Environ. Sci. Technol.* **1996**, *30* (1), 66–71.

(8) Henderson, A. D.; Demond, A. H. Long-term performance of zero-valent iron permeable reactive barriers: A critical review. *Environ. Eng. Sci.* **2007**, *24* (4), 401–423.

(9) Matheson, L. J.; Tratnyek, P. G. Reductive dehalogenation of chlorinated methanes by iron metal. *Environ. Sci. Technol.* **1994**, *28* (12), 2045–2053.

(10) Arnold, W. A.; Roberts, A. L. Pathways of chlorinated ethylene and chlorinated acetylene reaction with Zn(0). *Environ. Sci. Technol.* **1998**, *32* (19), 3017–3025.

(11) Johnson, T. L.; Scherer, M. M.; Tratnyek, P. G. Kinetics of halogenated organic compound degradation by iron metal. *Environ. Sci. Technol.* **1996**, *30* (8), 2634–2640.

(12) Scherer, M. M.; Balko, B. A.; Gallagher, D. A.; Tratnyek, P. G. Correlation analysis of rate constants for dechlorination by zero-valent iron. *Environ. Sci. Technol.* **1998**, *32* (19), 3026–3033.

(13) Lee, W. J.; Batchelor, B. Abiotic reductive dechlorination of chlorinated ethylenes by iron-bearing phyllosilicates. *Chemosphere* **2004**, *56* (10), 999–1009.

(14) Lee, W.; Batchelor, B. Abiotic reductive dechlorination of chlorinated ethylenes by iron-bearing soil minerals. 1. Pyrite and magnetite. *Environ. Sci. Technol.* **2002**, *36* (23), 5147–5154.

(15) Lee, W.; Batchelor, B. Abiotic, reductive dechlorination of chlorinated ethylenes by iron-bearing soil minerals. 2. Green rust. *Environ. Sci. Technol.* **2002**, *36* (24), 5348–5354.

(16) Lowry, G. V.; Reinhard, M. Hydrodehalogenation of 1- to 3-carbon halogenated organic compounds in water using a palladium catalyst and hydrogen gas. *Environ. Sci. Technol.* **1999**, *33* (11), 1905–1910.

(17) Butler, E. C.; Hayes, K. F. Kinetics of the transformation of trichloroethylene and tetrachloroethylene by iron sulfide. *Environ. Sci. Technol.* **1999**, *33* (12), 2021–2027.

(18) Burris, D. R.; Campbell, T. J.; Manoranjan, V. S. Sorption of trichloroethylene and tetrachloroethylene in a batch reactive metallic iron-water system. *Environ. Sci. Technol.* **1995**, *29* (11), 2850–2855.

(19) Valcárcel, A.; Clotet, A.; Ricart, J. M.; Illas, F. Comparative theoretical study of the structure and bonding of propyne on the Pt(111) and Pd(111) surfaces. *Chem. Phys.* **2005**, *309*, 33–39.

(20) Vanderbilt, D. Soft self-consistent pseudopotentials in a generalized eigenvalue formalism. *Phys. Rev. B* **1990**, *41* (11), 7892–7895.

(21) Perdew, J. P.; Burke, K.; Ernzerhof, M. Generalized gradient approximation made simple. *Phy. Rev. Lett.* **1996**, *77* (18), 3865–3868.

(22) Baroni, S.; Dal Corso, A.; de Gironcoli, S.; Giannozzi, P. Quantum ESPRESSO: opEn-Source Package for Research in Electronic Structure, Simulation, and Optimization, v. 3.2. http://www.pwscf.org/ 2007.

(23) Monkhorst, H. J.; Pack, J. D. Special points for brillouin-zone integrations. *Phys. Rev. B* **1976**, *13* (12), 5188–5192.

(24) Jiang, D. E.; Carter, E. A. Adsorption and diffusion energetics of hydrogen atoms on Fe(110) from first principles. *Surf. Sci.* **2003**, *547* (1−2), 85–98.

(25) Jiang, D. E.; Carter, E. A. Adsorption and dissociation of CO on Fe(110) from first principles. *Surf. Sci.* **2004**, *570* (3), 167–177.

(26) Kokalj, A. Computer graphics and graphical user interfaces as tools in simulations of matter at the atomic scale. *Comput. Mater. Sci.* **2003**, *28* (2), 155–168.

(27) (*Frisch, M. J.; Trucks, G. W.; Schlegel, H. B.; Scuseria, G. E.; Robb, M. A.; Cheeseman, J. R.; Montgomery, J. A., Jr.; Vreven, T.; Kudin, K. N.; Burant, J. C.; Millam, J. M.; Iyengar, S. S.; Tomasi, J.; Barone, V.; Mennucci, B.; Cossi, M.; Scalmani, G.; Rega, N.; Petersson, G. A.; Nakatsuji, H.; Hada, M.; Ehara, M.; Toyota, K.; Fukuda, R.; Hasegawa, J.; Ishida, M.; Nakajima, T.; Honda, Y.; Kitao, O.; Nakai, H.; Klene, M.; Li, X.; Knox, J. E.; Hratchian, H. P.; Cross, J. B.; Bakken, V.; Adamo, C.; Jaramillo, J.; Gomperts, R.; Stratmann, R. E.; Yazyev, O.; Austin, A. J.; Cammi, R.; Pomelli, C.; Ochterski, J. W.; Ayala, P. Y.; Morokuma, K.; Voth, G. A.; Salvador, P.; Dannenberg, J. J.; Zakrzewski, V. G.; Dapprich, S.; Daniels, A. D.; Strain, M. C.; Farkas, O.; Malick, D. K.; Rabuck, A. D.; Raghavachari, K.; Foresman, J. B.; Ortiz, J. V.; Cui, Q.; Baboul, A. G.; Clifford, S.; Cioslowski, J.; Stefanov, B. B.; Liu, G.; Liashenko, A.; Piskorz, P.; Komaromi, I.; Martin, R. L.; Fox, D. J.; Keith, T.; Al-Laham, M. A.; Peng, C. Y.; Nanayakkara, A.; Challacombe, M.; Gill, P. M. W.; Johnson, B.; Chen, W.; Wong, M. W.; Gonzalez, C.; Pople, J. A.*) *Gaussian 03, revision C.02*; Gaussian, Inc.: Wallingford, CT, 2004.

(28) Schaftenaar, G.; Noordik, J. H. Molden: a pre- and post-processing program for molecular and electronic structures. *J. Comput. Aided Mol. Des.* **2000**, *14* (2), 123–134.

(29) Miertus, S.; Tomasi, J. Approximate evaluations of the electrostatic free-energy and internal energy changes in solution processes. *Chem. Phys.* **1982**, *65* (2), 239–245.

(30) Soon, A.; Todorova, M.; Delley, B.; Stampfl, C. Oxygen adsorption and stability of surface oxides on Cu(111): A first-principles investigation. *Phys. Rev. B* **2006**, *73* (16), .

(31) Shih, H. D.; Jona, F.; Bardi, U.; Marcus, P. M. The atomic structure of Fe{110}. *J. Phys. C: Solid State* **1980**, *13* (19), 3801–3808.

(32) Spencer, M. J. S.; Hung, A.; Snook, I. K.; Yarovsky, I. Density functional theory study of the relaxation and energy of iron surfaces. *Surf. Sci.* **2002**, *513* (2), 389–398.

(33) Barbosa, L.; Loffreda, D.; Sautet, P. Chemisorption of trichloroethene on the PdCu alloy (110) surface: A periodical density functional study. *Langmuir* **2002**, *18* (7), 2625–2635.

(34) Bernardo, C.; Gomes, J. The adsorption of ethylene on the (110) surfaces of copper, silver and platinum: a DFT study. *J. Mol. Struct.: Theochem.* **2002**, *582*, 159–169.

(35) Kokalj, A.; Dal Corso, A.; de Gironcoli, S.; Baroni, S. DFT study of a weakly pi-bonded C_2H_4 on oxygen-covered Ag(100). *J. Phys. Chem. B* **2006**, *110* (1), 367–376.

(36) Itoh, K.; Kiyohara, T.; Shinohara, H.; Ohe, C.; Kawamura, Y.; Nakai, H. DFT calculation analysis of the infrared spectra of ethylene adsorbed on Cu(110), Pd(110), and Ag(110). *J. Phys. Chem. B* **2002**, *106* (41), 10714–10721.

(37) Watson, G. W.; Wells, R. P. K.; Willock, D. J.; Hutchings, G. J. Density functional theory calculations on the interaction of ethene with the {111} surface of platinum. *J. Phys. Chem. B* **2000**, *104* (27), 6439–6446.

(38) Bocquet, M. L.; Sautet, P.; Cerda, J.; Carlisle, C. I.; Webb, M. J.; King, D. A. Specific ethene surface activation on silver oxide covered Ag{111} from the interplay of STM experiment and theory. *J. Am. Chem. Soc.* **2003**, *125* (10), 3119–3125.

(39) Zheng, T.; Stacchiola, D.; Poon, H. C.; Saldin, D. K.; Tysoe, W. T. Determination of the structure of disordered overlayers of ethylene on clean and hydrogen-covered Pd(111) by low-energy electron diffraction. *Surf. Sci.* **2004**, *564* (1−3), 71–78.
(40) Zhang, N. L.; Luo, J.; Blowers, P.; Farrell, J. Understanding trichloroethylene chemisorption to iron surfaces using density functional theory. *Environ. Sci. Technol.* **2008**, *42* (6), 2015–2020.
(41) Somorjai, G. A. Modern surface science and surface technologies: An introduction. *Chem. Rev.* **1996**, *96* (4), 1223–1235.
(42) Barbosa, L.; Sautet, P. Trichloroethene dechlorination reactions on the PdCu(110) alloy surface: A periodical density functional theory study of the mechanism. *J. Catal.* **2002**, *207* (1), 127–138.
(43) Desai, S. K.; Pallassana, V.; Neurock, M. A periodic density functional theory analysis of the effect of water molecules on deprotonation of acetic acid over Pd(III). *J. Phys. Chem. B* **2001**, *105* (38), 9171–9182.
(44) Zolotoy, N. B. Estimate of the enthalpy change of proton hydration in water. *Dokl. Phys. Chem.* **2006**, *406*, 30–32.
(45) Becker, U.; Risthaus, P.; Bosbach, D.; Putnis, A. Selective attachment of monovalent background electrolyte ions and growth inhibitors to polar steps on sulfates as studied by molecular simulations and AFM observations. *Mol. Simul.* **2002**, *28* (6−7), 607–632.
(46) Scherer, M. M.; Balko, B. A.; Tratnyek, P. G., The role of oxides in reduction reactions at the metal-water interface. In *Kinetics and Mechanisms of Reactions at the Mineral−Water Interface*; Sparks, D. L., Grundl, T., Eds.; American Chemical Society: Washington, DC, 1999; pp 301−322.
(47) Lee, G. D.; Han, S. W.; Yu, J. J.; Ihm, J. Catalytic decomposition of acetylene on Fe(001): A first-principles study. *Phys. Rev. B* **2002**, *66* (8), .
(48) Dewar, M. J. S.; Ford, G. P. Relationship between olefinic pi-complexes and 3-membered rings. *J. Am. Chem. Soc.* **1979**, *101* (4), 783–791.
(49) Zaera, F. An organometallic guide to the chemistry of hydrocarbon moieties on transition metal surfaces. *Chem. Rev.* **1995**, *95* (8), 2651–2693.
(50) Sivavec, T. M.; Horney, D. P. *Reductive dechlorination of chlorinated ethenes by iron metal; 208th National Meeting, American Chemical Society, Anaheim, CA; Environmental Division Extended Abstracts*; American Chemical Society: Washington, DC, 1995; p 695.

ES802523A